(Received 12 April 2025, Accepted 3 June 2025, Scheduled 15 June 2025)

Study of Complex Shapes Reflective Structures for UWB Antenna Based on Dielectric Materials with Various Conductive Coatings

Mikhail S. Shishkin[1, 2, *]

[1] Science and Research Department, Moscow Technical University of Communication and Informatics, Moscow, Russia
[2] Engineering School of Information Technologies, Telecommunications and Control Systems
Ural Federal University named after the first President of Russia B. N. Yeltsin, Yekaterinburg, Russia

ABSTRACT: The paper summarizes the principles of various reflectors for microstrip antennas with a particular focus on volumetric reflectors (cavities) that are more challenging to manufacture than flat structures made from printed circuit boards or sheet metal. It is demonstrated in this study that volumetric reflectors can significantly enhance the directional properties of an antenna without typically increasing the antenna's radiating area or overall volume. To reduce the manufacturing costs associated with antenna's volumetric parts, the article proposes the use of 3D printing with commonly available dielectric materials, such as plastics. This technique is relatively straightforward and cost-effective compared to the manufacture of volumetric metal parts. Moreover, the article suggests applying a conductive layer to the parts of the antenna that contribute to radiation formation. The option of covering the reflector (cavity) on the inside with ordinary aluminum foil and the option with conductive enamel are considered. The results of simulation in antenna designs with different reflector conductivities and the results of experimental studies of antennas are presented. The results obtained show that the method is feasible to be used with virtually no compromise on the antenna characteristics and substantially reduces the production cost.

1. INTRODUCTION

Today, antenna technologies are advancing at an accelerating pace. Increasingly complex antenna designs with various characteristics are emerging. Research is ongoing to enhance the operating bandwidth of both omnidirectional and unidirectional antennas, as well as to improve their polarization properties [1–10]. Methods are being studied to improve the antenna performance by integrating them into antenna arrays [11–15]. The need for manufacturing accuracy usually rises with the advancement of antenna designs, both for the antennas themselves and for their component parts.

Achieving high antenna performance can be accomplished through various methods. For example, utilizing high-Q substrates, such as air substrates or suspended substrates, for microstrip antennas can significantly boost the gain when the exciter is optimally placed above a flat conductive screen (reflector) [2, 8–10, 14, 15]. Expanding the operating frequency range can be achieved through various cutouts in the antenna exciters or by optimally arranging active and passive elements within a single radiating structure [9, 10, 16, 17]. To enhance the antenna's matching or radiating characteristics, specific antenna (active exciter) excitation techniques are utilized [2, 5, 18–27].

Manufacturing the entire structure or any of its individual components, in the case of microstrip antennas, is quite simple and is recommended to a large extent. The production of printed elements using a dielectric substrate is typically accomplished through using standard etching methods, either manually or with special equipment. On the contrary, without a dielectric substrate (using air as the substrate), the antenna elements are most commonly made of sheet metal by means of laser cutting. Fastening of the antenna elements is performed by means of metal or dielectric racks or screws.

Often, radiating antenna elements, especially when we are talking about microstrip antennas or similar structures, are made volumetric; sometimes this serves to expand the operating frequency bandwidth of an antenna or to improve its radiation performance. The most well-known volumetric structures in the world of antennas, if we are not limited to microstrip (or printed) elements, are horn or parabolic reflector antennas. While the techniques used in this article are quite suitable for these types of antennas, we will restrict our consideration to microstrip antennas or antennas with a structure similar to the microstrip [18–30].

This article discusses volumetric reflectors (cavities) used in microstrip antennas and how the authors have significantly enhanced the performance of these antennas across wide and ultrawide radio frequency ranges. Commonly, such reflectors are shaped like a box, with edges intersecting at right angles (a cuboid with a cutout for the placement of radiating elements). However, more complex forms of cavities (resonators) also exist, marked by inclined walls or walls of various shapes, as well as differently shaped cutouts [31–49]. Volumetric reflectors

* Corresponding author: Mikhail S. Shishkin (mikkhail666@gmail.com).

are significantly more challenging to manufacture than all other parts of a microstrip antenna, regardless of the type of dielectric substrate used (including air substrate). Producing these elements from metal with high precision incurs significant costs. Although technologies for 3D printing with metal materials are available, the overall costs of production remain expensive.

In this article, we examine the possibility of manufacturing a volumetric reflector with a complex shape using a cavity-backed antenna from [49] as a case study. The reflector may be constructed from plastic and then coated with conductive materials, particularly aluminum foil and a paint containing a silver additive.

2. CAVITY-BACKED ANTENNAS FEATURES

Cavity-backed antennas have been known for over 50 years, and the fundamentals of their operation were previously suggested and discussed during that time, using slot antennas as an example [50–52]. The essence of the operation of these antennas arises from the fact that the field distribution at the exciter (in this case, the radiating slot) depends on the excitation of higher modes of the cavity, as well as the principal mode (TE_{10}). The example of a common equivalent circuit for a cavity-backed antenna is illustrated in Figure 1. In the circuit, the shunt conductance acts as the radiation conductance of the exciter (either a slot or patch), while covering radiation, conductor, and dielectric losses. The parallel susceptance is the sum of the shunt susceptance of the exciter (L_eC_e) and the cavity susceptance in the TE mode ($L_{cTE}C_c$). The series resonant circuit (L_{cTM}) here is the result of the energy stored in the TM modes within the cavity, where the cavity resonances are defined as follows:

$$f_r = \frac{c}{2\sqrt{\varepsilon_r \cdot \mu_r}} \cdot \sqrt{\left(\frac{m}{a}\right)^2 + \left(\frac{n}{b}\right)^2}, \qquad (1)$$

where μ_r is the relative permeability, and ε_r is the relative permittivity of the cavity-filling material (for air, $\mu_r = 1$ and $\varepsilon_r = 1$); m and n are the numbers of half-cycle field variations along the dimensions a and b of the cavity, respectively; c is the velocity of electromagnetic wave propagation in vacuum.

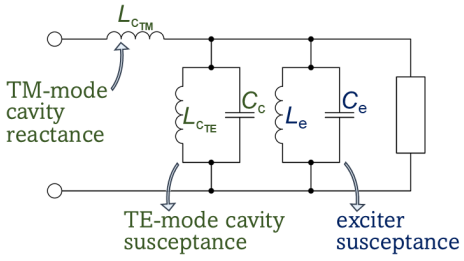

FIGURE 1. The equivalent circuit of a cavity-backed exciter.

An increased radiation conductance of the slot is achieved due to a cavity with sufficiently large dimensions, as the energy stored in the cavity near the slot predominantly is in the TE_{10} mode. However, according to [49], small cavities also enhance the field distribution of an exciter.

There are more complex designs of cavity-backed slot antennas, as shown in [31–32], which propose waveguide-fed antenna arrays. Microstrip antennas function similarly, with the exciter being a patch of a specific shape rather than a slot, while the cavity provides improved field distribution over its surface. In the simplest case, patches of a rectangular shape or, with minor modifications, cuboid cavities similar to those of slot antennas are used [33–36]. More complex forms of exciters are also utilized, allowing the authors to improve the impedance matching bandwidth of the antenna or to enable the antenna to operate in several polarizations or circular polarizations [37–40]. In all these designs, cuboid cavities are used.

The cavity-backed antennas under consideration present considerable manufacturing challenges. The cavity is made from metal and has a volumetric shape, which requires specialized metal processing equipment. In addition, high accuracy is often required in the fabrication of such designs, which significantly increases the cost of the antenna, whether produced as a single unit or in mass production. Moreover, the inclusion of metal parts considerably increases the weight of the antenna, which sometimes can be a crucial factor. To avoid the use of metal parts, some researchers have proposed designs for multilayer printed circuit board (PCB) antennas that use a cavity structure based on metallized vias placed at close intervals [41–43].

There are also options for cylindrical-shaped cavities in microstrip antennas. Usually, these cavities are used for printed spiral or log-periodic wideband (WB) and ultra-wideband (UWB) designs [44–45]. However, other antenna designs featuring cylindrical cavities have also been proposed; examples of such designs can be found in [46–47]. In the case of a cuboid cavity, multilayer PCBs with metallized holes are used to form a cylindrical cavity. An example of such an antenna is provided in [48]. A cylindrical cavity similarly enhances the radiation characteristics by improving the field distribution on the antenna's radiating elements; however, it is more commonly used for circularly polarized antennas.

Let us consider examples of designs from [49], where the pyramidal shapes of cavities significantly improved the efficiencies of wideband [9] and UWB [10] antennas. This improvement in the radiation characteristics was reached without increasing the total volume of the antennas. First, let us focus on an example of the wideband antenna from [9]. The transformation of its design from a flat reflector to an inverted pyramidal cavity resulted in an improvement in an antenna efficiency of up to approximately 10%, with the gain increasing by up to 1 dB over a wide frequency range — more than 35% fractional bandwidth (4600–6200 MHz). It is noteworthy that the radiation performance of the antenna was not significantly enhanced by the cuboid cavity, as results from the simulation shown in [49]; for example, the aperture efficiency was merely increased by only 2–4%, and the gain was only boosted from 0.1 to 1 dB in the operating frequency band of the antenna. In addition, when using a cuboid reflector (cavity), the gain improvement occurs unevenly over the entire operating frequency range, with a more noticeable effect towards the edges rather than in the center in comparison with a pyramidal cavity.

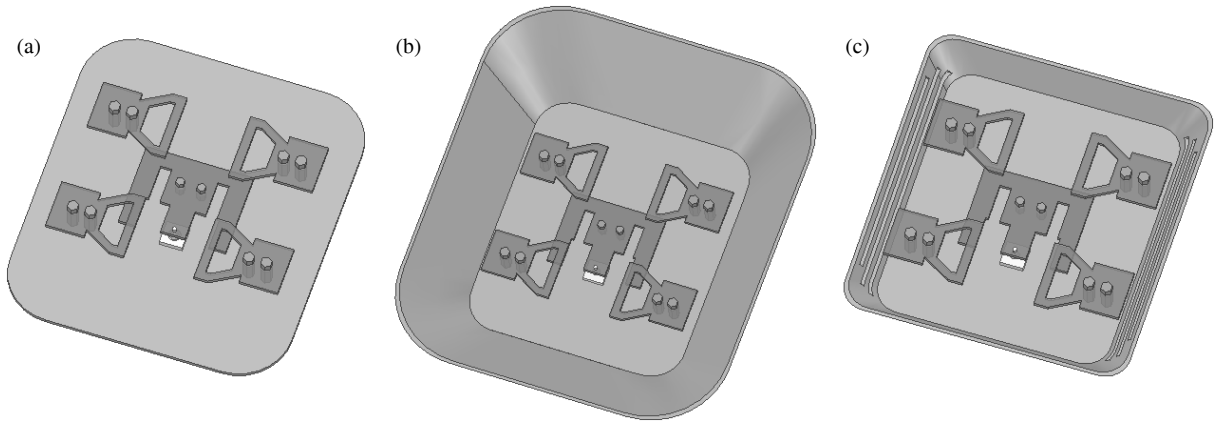

FIGURE 2. The studied UWB antenna: (a) an original antenna from [10]; (b) an antenna with the large-sized pyramidal cavity; (c) an antenna with the ridged small-sized pyramidal cavity.

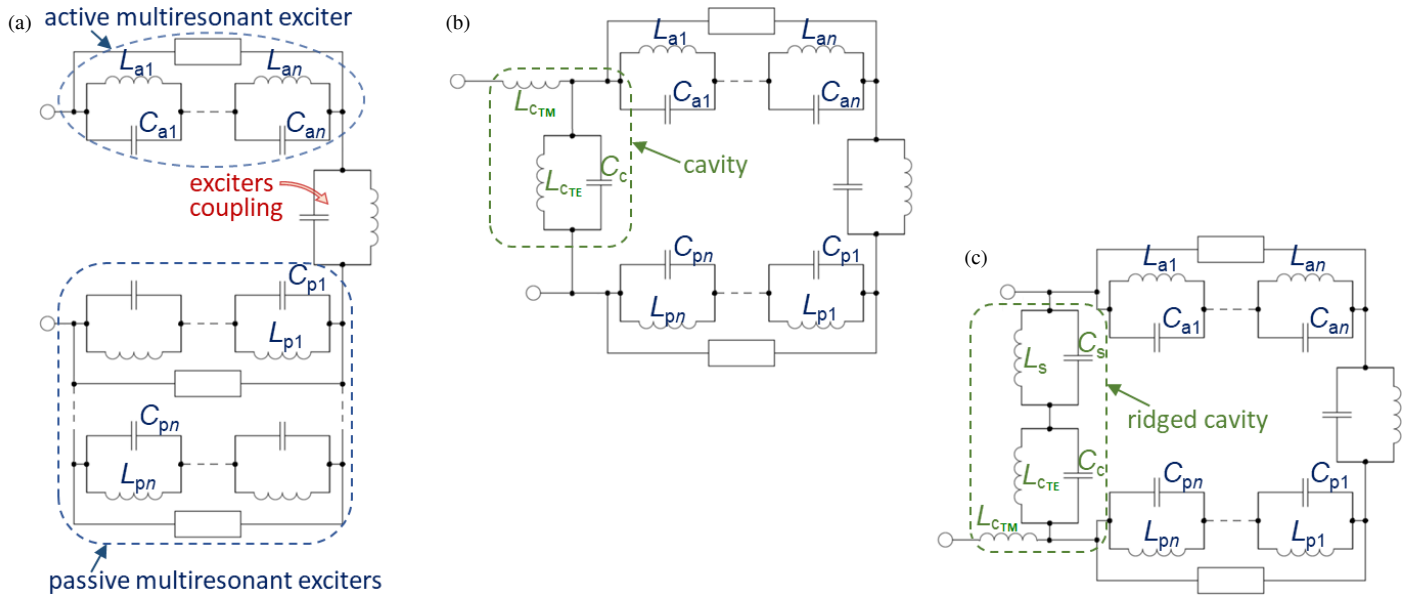

FIGURE 3. The equivalent circuits of the studied UWB antenna: (a) an original antenna from [10]; (b) an antenna with a large-sized pyramidal cavity; (c) an antenna with a small-sized ridged pyramidal cavity.

We will consider the UWB antenna from [10] in light of the simulation results given in [49]. The use of a pyramidal cavity with slots cut into the side walls against a flat reflector made it possible to increase an antenna's efficiency up to about 20% (the gain increased from 1 to 3 dB in the operating band) over an ultrawide frequency range — more than 100% bandwidth (3.9–11 GHz). However, the cuboid cavity provided a substantially greater improvement in the antenna's radiation performance: the gain upgraded from 0.3 to 1 dB in the operating frequency range, and the aperture efficiency increased by 5–10%.

We will then examine the options of the only UWB antenna, as this allows us to investigate a fairly wide frequency range, about between 3.5 and 11 GHz. In this case, we will think about designing the cavity in a pyramidal shape. According to the previous studies [49], it is obvious that this design allows us to achieve greater efficiency, although the complexity of such a cavity still makes it difficult to create. Figure 2 shows the possible design options for the UWB antenna that is being studied, which contains a full metal reflector (cavity): (a) an original antenna from [10] presented for comparison with cavity-backed designs; (b) an antenna with a large-sized cavity with inverted-pyramidal form; (c) an antenna with a ridged small-sized inverted-pyramidal cavity.

Figure 3 illustrates the common equivalent circuits of the antennas under study. The circuit corresponding to the original design [10] consists of several serial L_aC_a circuits corresponding to a multi-resonant active exciter. Similarly, the passive elements are represented as parallel blocks of serial multi-resonance L_pC_p circuits. The connections between the active and passive exciters are carried out through electromagnetic coupling and metallic vias, as shown in circuit (a) in Figure 3. By adding an inverted pyramidal cavity, we see a significant improvement in the E-field distribution on the radiating elements (Figure 4(b)) compared to the original antenna

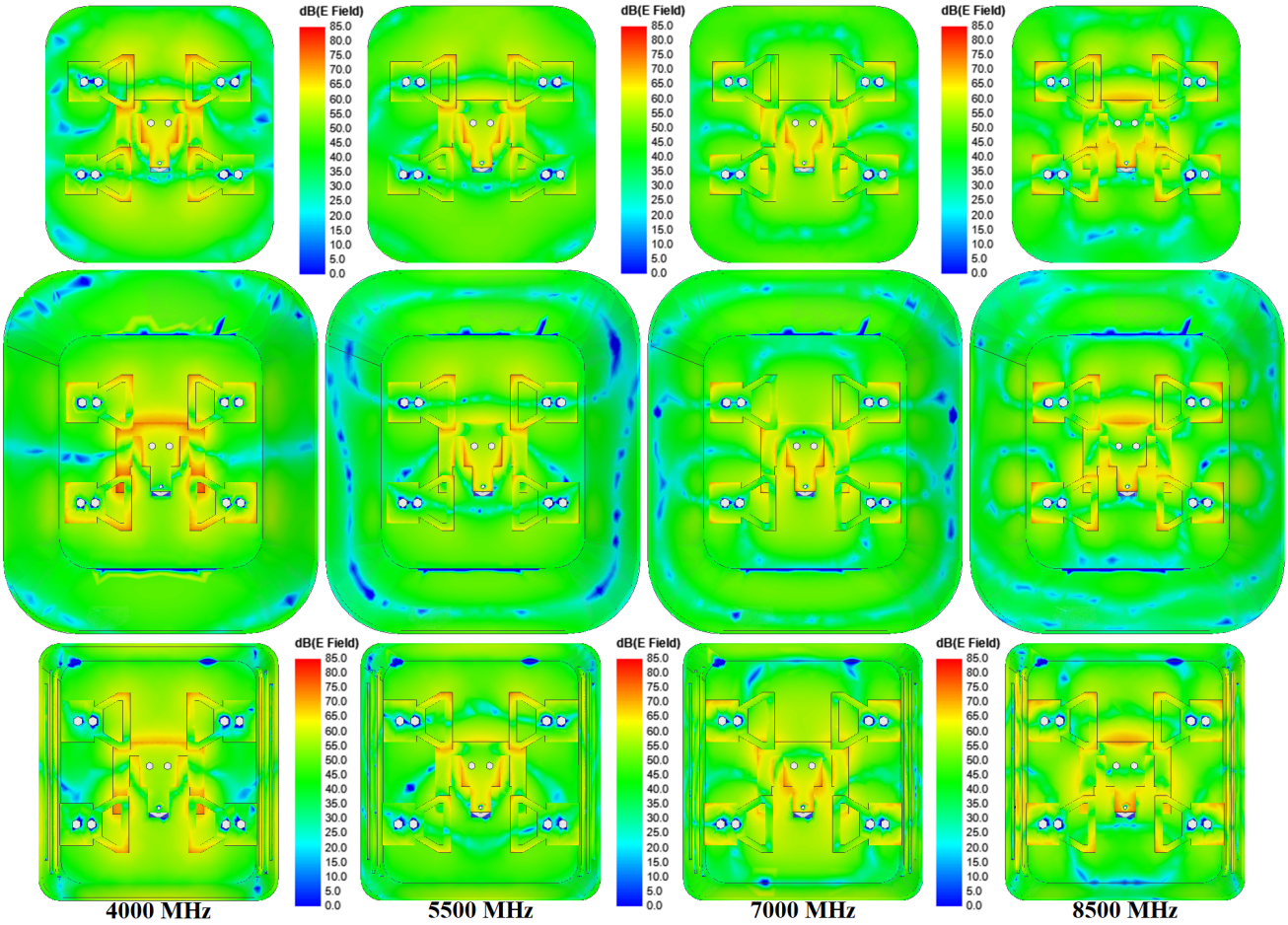

FIGURE 4. The E-filed distribution on the surfaces of the studied UWB antenna elements at frequencies ranging from 4000 to 8500 MHz: (a) an original antenna from [10]; (b) an antenna with a large-sized pyramidal cavity; (c) an antenna with a small-sized ridged pyramidal cavity.

design (Figure 4(a)). In the equivalent circuit, we can show this in the form of an $L_{\text{cTM}}L_{\tilde{\text{n}}\text{TE}}C_{\tilde{\text{n}}}$ circuit connected in parallel to the multi-resonant structure of the antenna (Figure 3(b)). Such a cavity is essentially an expanding rectangular waveguide (waveguide-based cavity), where, unlike a rectangular cross-section, a much larger number of modes can fit, the frequencies of which can be conditionally limited to the following values:

$$\begin{cases} f_{r_{\min}} = \dfrac{c}{2\sqrt{\varepsilon_r \cdot \mu_r}} \cdot \sqrt{(m/a_{\min})^2 + (n/b_{\min})^2} \\ f_{r_{\max}} = \dfrac{c}{2\sqrt{\varepsilon_r \cdot \mu_r}} \cdot \sqrt{(m/a_{\max})^2 + (n/b_{\max})^2} \end{cases}. \quad (2)$$

Variant (b) in Figure 2 is larger than the original design presented in [10], which increases the antenna gain but reduces radiation efficiency. To further increase the gain, this design can be transformed into a horn antenna, as illustrated, for example, in [53]. However, to improve the aperture efficiency, the antenna size should not increase, which was studied in detail in [49]. In this study, we use a cavity with an area equal to that of the reflector in the original design (Figure 2(a)), while maintaining the tendency of expanding the walls from the bottom to the top. According to condition (2), such a cavity will not provide an effective improvement in antenna performance across the entire frequency range. Therefore, resonant length slots (either half or a quarter of the wavelength at the required frequency) are introduced into the design, cut into the side walls of the cavity (Figure 2(c)). In Figure 4(c), we observe that the cavity, similar to variant (b), amplifies the radiation of the antenna, improving the distribution of the E-field on the radiating elements. However, it is also evident that the radiation is generated in the slots. In the equivalent circuit, we designate this as an additional circuit $L_{\text{s}}C_{\text{s}}$ (Figure 3(c)).

3. CAVITY-BACKED ANTENNAS LOSSES

In all circuits depicted in Figure 3, resistor symbols are used to show the presence of various types of losses, including resistive (conductive) losses in metal parts, dielectric losses (losses in air), and radiation losses. This study emphasizes the importance of conductive losses, which can be quantified (in dB) for a microstrip transmission line (MTL) segment of length l and width w, with the distance between a stripline and a ground plane h, and can be defined as the sum of the losses occurring directly in the line (strip) and the losses in the ground plane [54–

56]:

$$L_c = L_l + L_g = 8.686 \cdot l \cdot \frac{R_l + R_g}{2Z}, \tag{3}$$

where Z is the MTL impedance:

$$\begin{cases} Z = \dfrac{60}{\sqrt{\varepsilon_{re}}} \cdot \ln\left(\dfrac{8h}{w} + 0.25\dfrac{w}{h}\right), \text{ for } \dfrac{w}{h} \le 1 \\ Z = \dfrac{120\pi}{\sqrt{\varepsilon_{re}}} \cdot \left[\dfrac{w}{h} + 1.393 + \right. \\ \quad \left. + 0.677 \ln\left(\dfrac{w}{h} + 1.444\right)\right]^{-1}, \text{ for } \dfrac{w}{h} \ge 1 \end{cases}, \tag{4}$$

R_l and R_g are the effective series resistance per unit length of the stripline conductor and ground plane, respectively:

$$R_l = \frac{1}{\Delta_l \cdot \sigma_l \cdot w}, \tag{5}$$

$$R_g = \frac{1}{\Delta_g \cdot \sigma_g \cdot w}, \tag{6}$$

where Δ_l and Δ_g are the skin depths, and σ_l and σ_g are the conductivities of the stripline and ground plane, respectively.

The effective substrate permittivity ε_{re} can be determined according to the approximation [54–56]:

$$\varepsilon_{re} = \frac{\varepsilon_r + 1}{2} + \frac{\varepsilon_r - 1}{2} \cdot \left(1 + \frac{10 \cdot h}{w}\right)^{-1/2}, \tag{7}$$

and for the air substrate (cavity filling) with relative permittivity $\varepsilon_r = 1$, effective permittivity $\varepsilon_{re} = 1$.

As is known, the depth of current penetration (m) depends on the frequency of wave oscillations f and the conductivity of the conductor (skin depth) [54–56]:

$$\Delta = \frac{1}{\sqrt{\pi \cdot \mu_0 \cdot \mu_r \cdot f \cdot \sigma}}, \tag{8}$$

where μ_0 is the magnetic constant ($\mu_0 = 4\pi \cdot 10^{-7}$); μ_r is the relative magnetic permeability of the conductor.

In the structures under study, the radiating elements are assumed to be made of sheet metal. When each radiating element is examined, it consists of series-connected MTL segments of different widths w_s and lengths l_s. Consequently, the losses at the exciter can be defined as the sum of the losses in the segments of the individual lines that comprise the exciter structure:

$$L_{exciter} = \sum L_s = 4.343 \cdot \sum l_s \cdot \frac{R_s}{Z_s}. \tag{9}$$

Let us consider the structure of the cavity (Figure 5). The frame itself is supposed to be manufactured using 3D printing technology from a dielectric material (for example, the ABS plastic). One side (the inner side facing the exciters) of the cavity is covered with a layer of conductive materials: the foil with $\sigma \approx 40 \times 10^6$ Siemens/m and the special mixture with

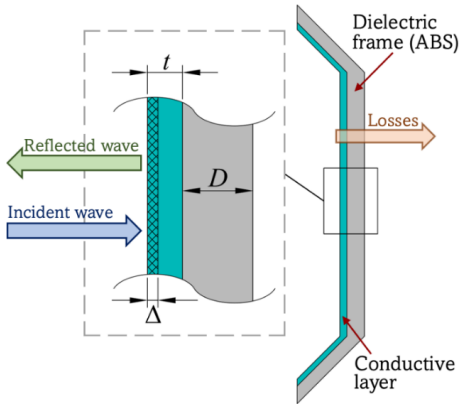

FIGURE 5. The appearance of the cavity construction.

$\sigma \approx 5 \times 10^6$ Siemens/m. In this study, the mixture consisting of epoxy resin and silver powder in a ratio of 10/1 is used.

The electromagnetic wave from the exciters falls towards the cavity surface (Figure 5), and, penetrating to the depth of the skin layer, is reflected towards the exciters, thereby improving the distribution of the E-field on their surfaces (which we saw in Figure 4). It is obvious that when the skin depth Δ exceeds the thickness of the conducting layer t, part of the power will pass through the cavity wall and will be radiated from the side opposite to the direction of the main radiation. We will consider this radiation as losses. It is understood that at $t > \Delta$ these losses can be avoided; however, in some papers [56–57] it is shown that such losses of different levels exist practically at any conductor thickness, while an optimal minimum ratio is proposed, after which the re-radiation losses stop rising:

$$\frac{t}{\Delta} \ge \frac{\pi}{2}. \tag{10}$$

Thus, understanding the skin depth is important when designing antennas with elements made from a thin conductive layer. Figure 6 shows the frequency dependence of skin depth for various conductivity values, where $\sigma \approx 60 \times 10^6$ corresponds to the parameters of copper. The provided graphs demonstrate that using either foil or the copper layer, the skin depth is practically the same, between 0.5 and 1.5 μm in the

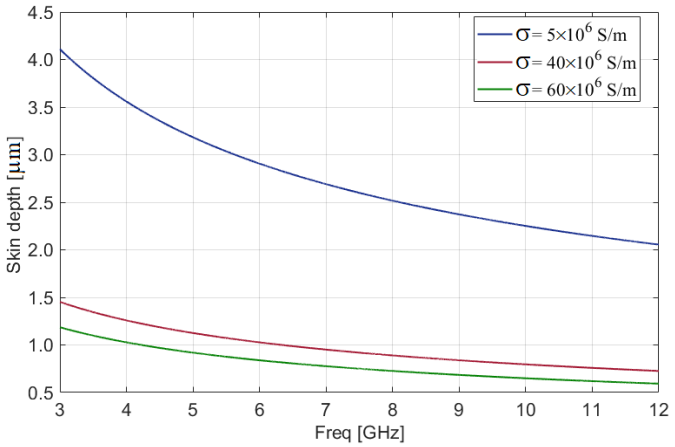

FIGURE 6. The frequency dependence of the skin depth at various conductivity values.

studied frequency range from 3 to 12 GHz. In contrast, using the proposed conductive mixture (enamel), the skin depth increases between 2 and 4 μm in the studied frequency range. It is assumed that 0.2 mm will be the foil thickness and that the enamel is applied in a layer thickness of 0.2 to 0.5 mm, which, in accordance with Figure 6, satisfies condition (10).

An essential problem remains the losses in the conductor, specifically within the depth of the skin layer. These losses are calculated in accordance with (3) and shown in Figure 7, where the solid line indicates a section of $10 \times 10\,\text{mm}^2$ at a height of 5 mm, and the dotted line corresponds to a section of $100 \times 100\,\text{mm}^2$ at a height of 5 mm. It is recommended to estimate the ohmic losses in the reflector (cavity) at the places where the E-field is most concentrated (for example, as shown in Figure 4). Therefore, it can be concluded that the use of conductive enamel will have a minimal impact on losses, which will amount to no more than 2–3% compared to copper.

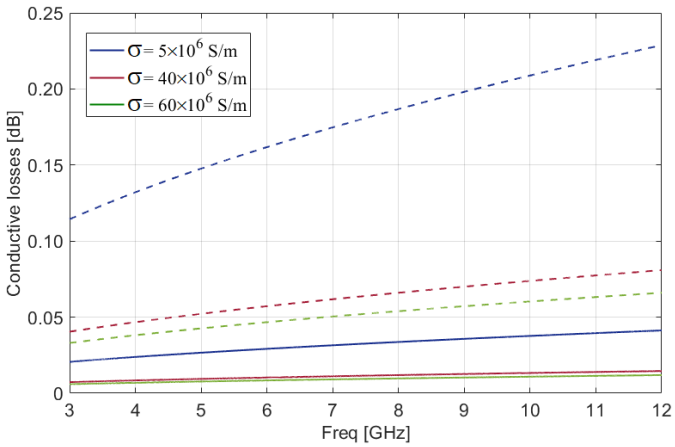

FIGURE 7. The frequency dependence of the ohmic losses for different conductivity values (solid line: $w = 10\,\text{mm}$, $l = 10\,\text{mm}$, $h = 5\,\text{mm}$; dotted line: $w = 100\,\text{mm}$, $l = 100\,\text{mm}$, $h = 5\,\text{mm}$).

4. CAVITY-BACKED ANTENNA SIMULATION

The 3D simulation of the studied cavity-backed antennas is performed using ANSYS EM Suite (HFSS Design) in order to perform a preliminary assessment of their characteristics. In the model, all radiating elements and mounting racks are represented as solid parts, which are assigned properties corresponding to metal. The cavity model consists of two layers: the outer layer, measuring 2 mm in thickness and having the properties of ABS-plastic (dielectric), and the inner layer, with a thickness of 0.2 mm, is assigned the parameters of the conductor.

4.1. UWB Antenna with Large-Sized Cavity

The model of the studied UWB antenna with a large-sized two-layer cavity is illustrated in Figure 8. Figures 9 and 10 show the results of simulations for the antenna. From the plots presented in Figure 9, it can be concluded that antenna gains for a solid metal and a dielectric cavity with various conductive layers on its surface have the same nature—the curves are almost indistinguishable. More significant differences between

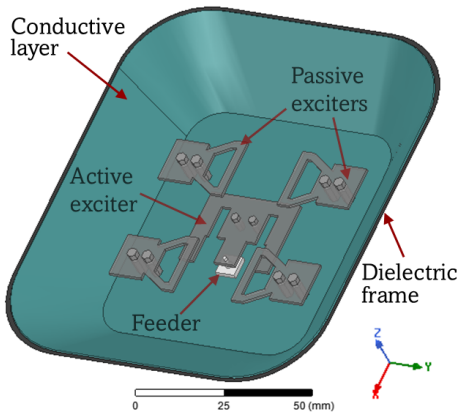

FIGURE 8. The studied UWB antenna model with a large-sized two-layer cavity.

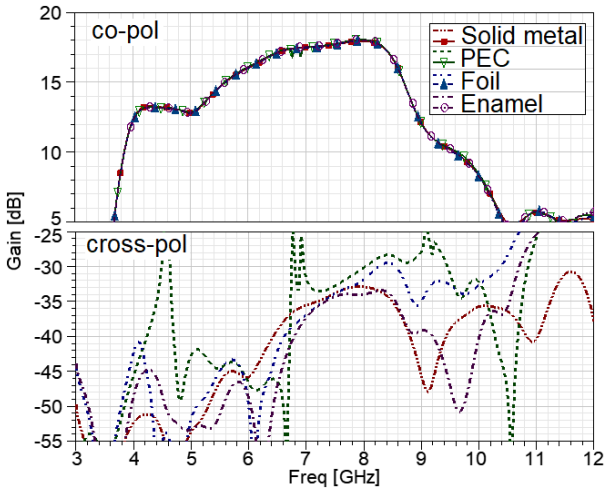

FIGURE 9. The simulated gain plots of the studied UWB antenna with a large-sized cavity.

the curves can be seen in Figure 10 on the aperture efficiency plots. However, even there, differences do not surpass 1%. The latter could be a result of calculation errors. Although the performance of all curves is typically similar, gain curves of cross-polarized variations surpass those of the main polarization; in certain places, the difference in values exceeds 10 dB. Given the relatively thin conductor layer, we presume that there is likely a calculation error.

Thus, based on the analysis of the obtained simulation results, it can be concluded that the proposed technique for manufacturing cavities using metal foil or conductive enamel can be applied while maintaining the antenna characteristic values in the entire operating frequency range.

4.2. UWB Antenna with Small-Sized Ridged Cavity

The model of the studied UWB antenna with a small-sized two-layer ridged cavity is shown in Figure 11. Figures 12 and 13 show the simulated frequency dependencies of the antenna's gain and efficiency, considering various conductive parameters of the cavity. As observed in the previous case, the gains of the antenna with a solid metal cavity and a dielectric cavity covered with various conductive layers show identical characteris-

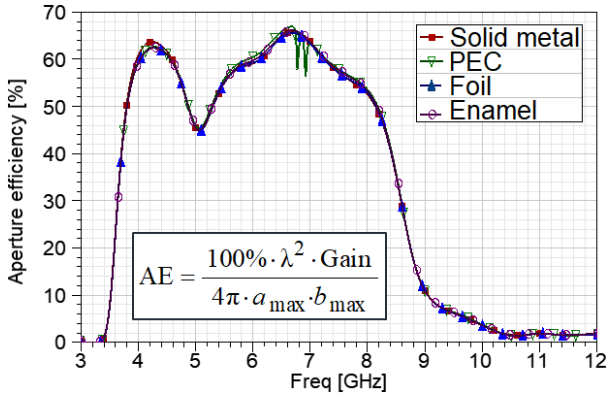

FIGURE 10. Simulated aperture efficiency plots for the studied UWB antenna with a large-sized cavity.

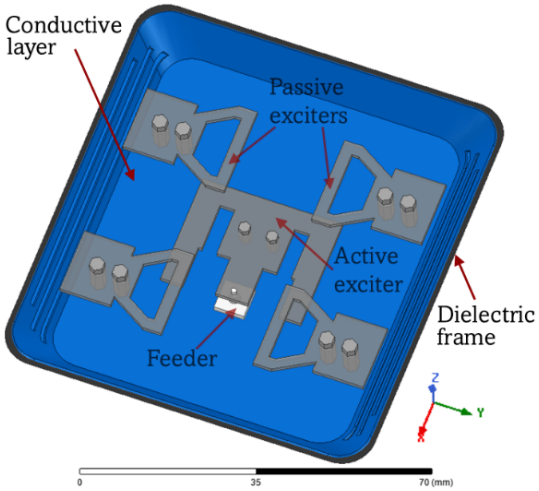

FIGURE 11. The studied UWB antenna model with a small-sized two-layer cavity.

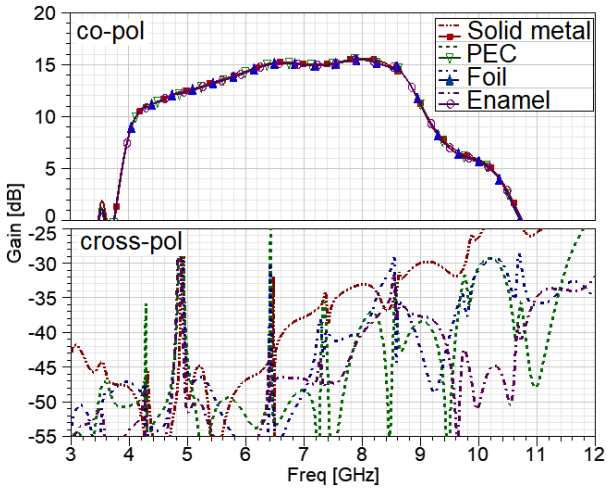

FIGURE 12. The simulated gain plots of the studied UWB antenna with a small-sized ridged cavity.

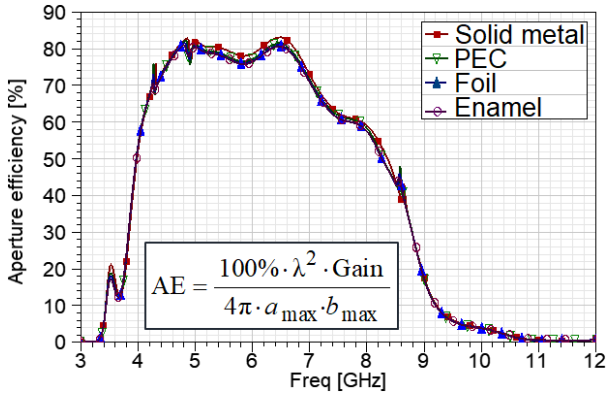

FIGURE 13. Simulated aperture efficiency plots for the studied UWB antenna with a small-sized ridged cavity.

tics; the curves are practically indistinguishable. More noticeable differences can be found in Figure 13, which shows the aperture efficiency plots. These differences are slightly greater than those in Figure 10 but do not exceed 3%, which may be associated with calculation errors of the thin layer. The cross-polarized gain curves show a character similar to the previous type of antenna; the shapes of all curves for the two-layered cavity antenna are generally alike. It should be pointed out that the curves are different in the range of high gain above 10 dBi (4–9 GHz), with variations of up to 10 dB compared to the solid-metal cavities. This difference is attributed to the presence of slots, which, unlike the previous design, are covered with a conductive layer only on the interior side.

Thus, both antenna variants demonstrate the possibility of using a dielectric frame coated with a conductive layer based on foil or enamel.

5. CAVITY-BACKED ANTENNA MEASUREMENTS

To evaluate the characteristics of antennas with different conductive coatings, prototypes were developed, and corresponding measurements were performed. In this section, we will discuss the results obtained and the manufacturing features of the structures studied.

5.1. UWB Antenna with a Large-Sized Cavity

When an antenna is manufactured, the cavity frame is initially constructed of plastic materials, such ABS or PETG. In the experiment, frames were manufactured using fused deposition modeling (FDM) technology (Figures 14(a) and (b)) and stereolithography (SLA) technology (Figure 14(c)). A thin layer of foil is then applied over the frame with a specialized glue (any glue ensures sticking of foil onto plastic proper), as shown in Figure 14(b); or a thin layer of conductive enamel is applied, as shown in Figure 14(c). Before further installation, it is necessary to allow sufficient time for the enamel and glue to cure in accordance with the technical manual. SLA technology allows for obtaining higher wall accuracy with minimal unevenness compared to FDM, making it the preferred technique for enamel application. In the case of FDM, smooth surfaces of cavities can be achieved using foil. Once the glue (or enamel) has cured, the active and passive exciters are mounted on the conductive surface using metal (brass) and dielectric (nylon) mounting racks, as implemented in the original design in [10],

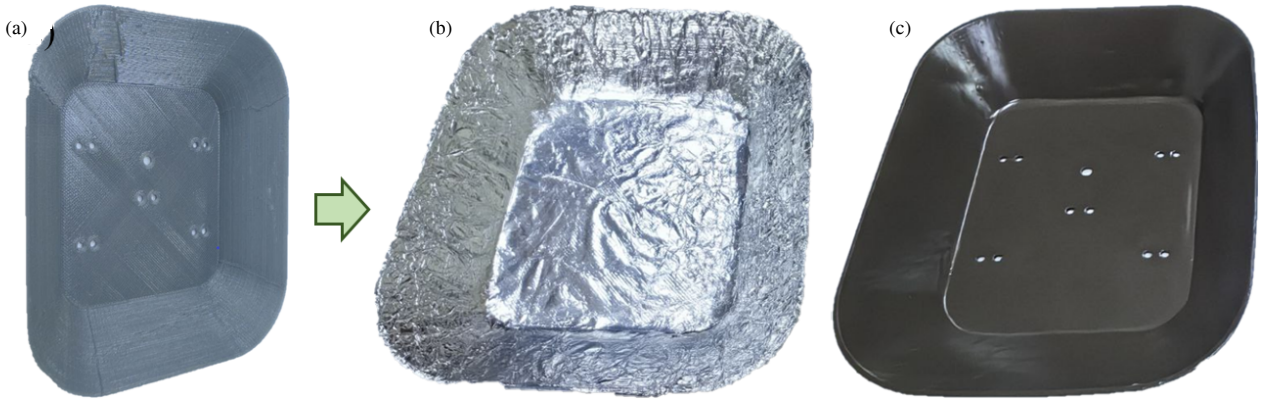

FIGURE 14. The manufactured large-sized cavity of the studied UWB antenna: (a) a plastic frame for the cavity; (b) a plastic frame with a foil coating; (c) a plastic frame with an enamel coating.

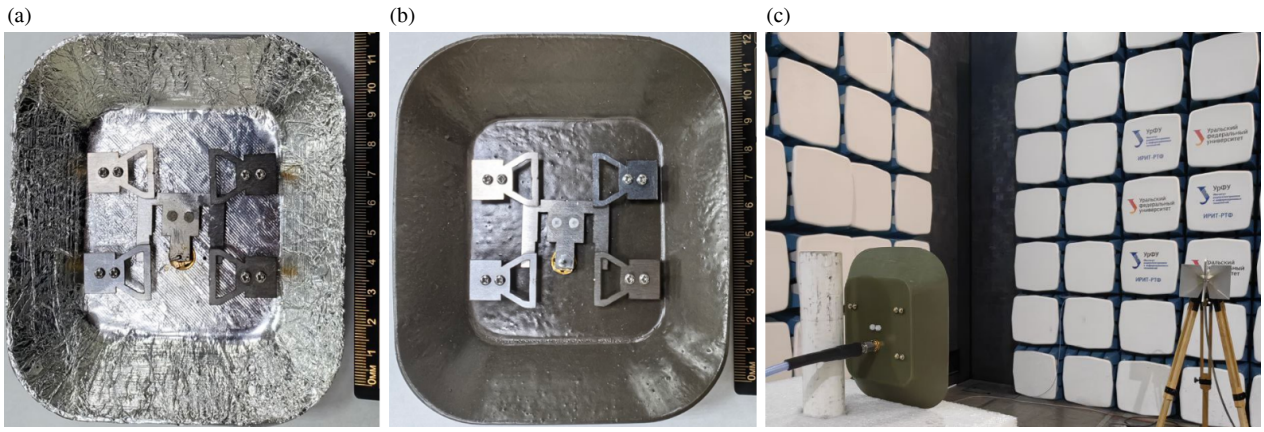

FIGURE 15. The studied UWB antenna prototypes with a large-sized cavity: (a) an antenna with a plastic cavity coated with foil; (b) an antenna with a plastic cavity coated with enamel; (c) the antenna measurements in an anechoic chamber.

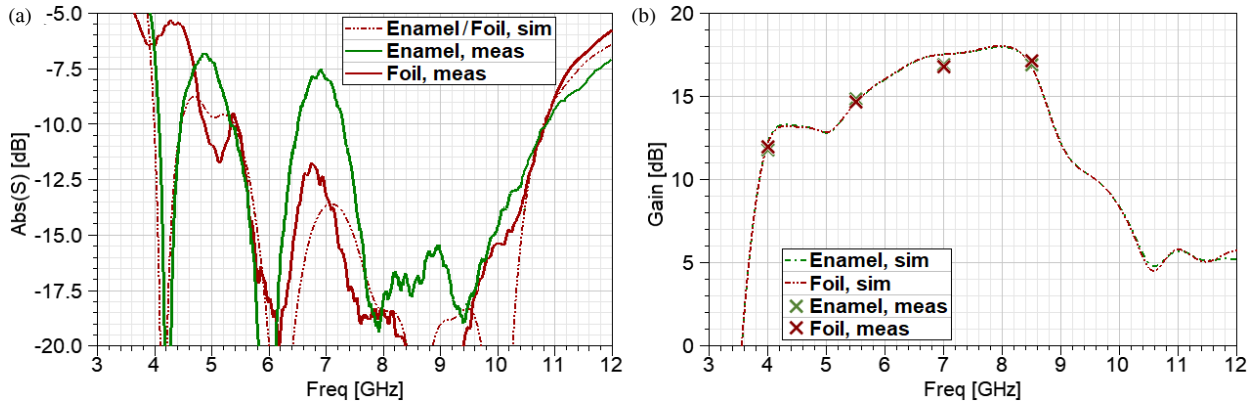

FIGURE 16. Results obtained from the study of the UWB antenna with a large two-layer cavity: (a) plots of the measured and the simulated reflection coefficient; (b) the measured and simulated gain plots.

and a connector (SMA) is installed at the antenna input (Figure 15).

For the manufactured prototypes with foil (Figure 15(a)) and enamel (Figure 15(b)) coatings, we measured the frequency dependence of the reflection coefficient modules (Figure 16(a)) at the antenna inputs ($|S_{11}|$), the gain values (Figure 16(b)) in the studied frequency range, and the radiation patterns (Figure 17) at frequencies of 4.0, 5.5, 7.0, and 8.5 GHz using an anechoic chamber (Figure 15(c)). The curves in Figure 16(b) make it evident that the antenna gain almost corresponds to the values obtained during simulation, with a difference not exceeding 0.5 dB. The antenna matching (Figure 16(a)) also corresponds

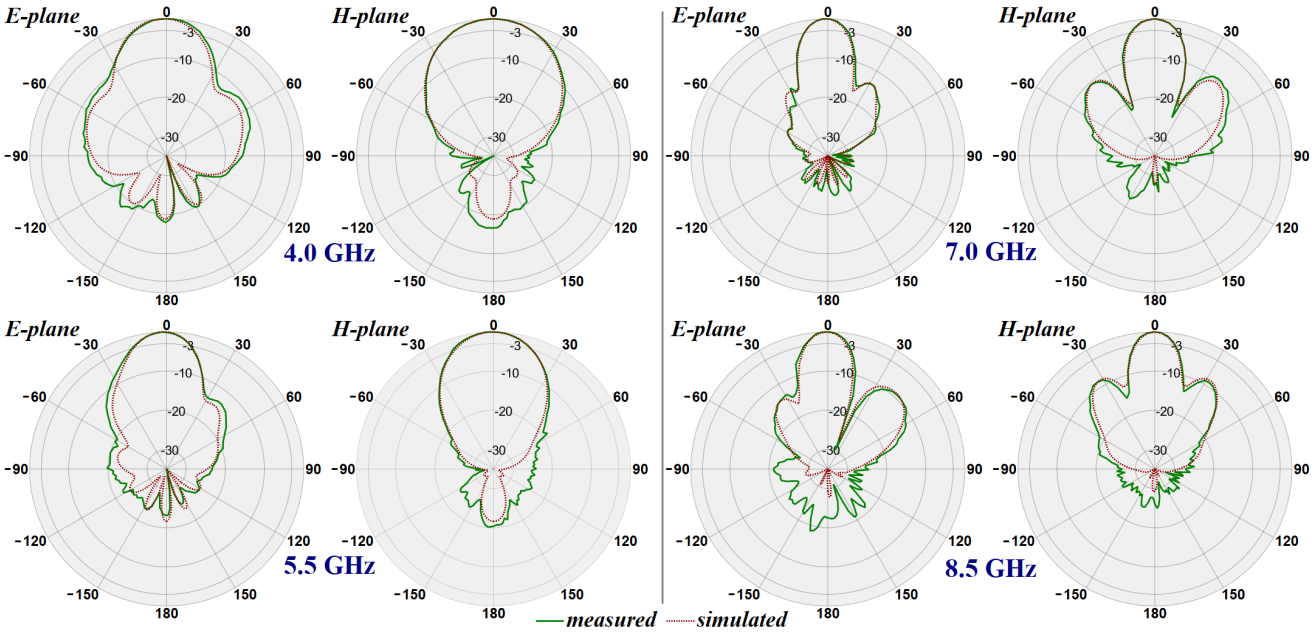

FIGURE 17. Radiation patterns of the proposed ultrawideband large-sized two-layer cavity antenna with enamel coating.

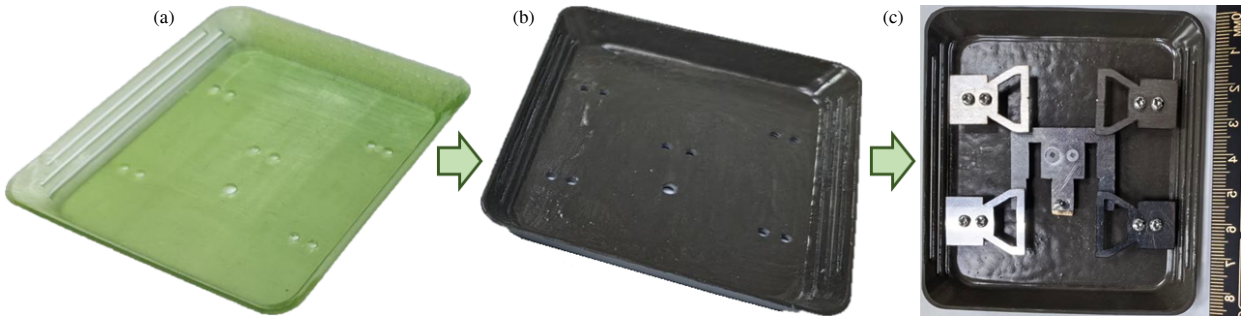

FIGURE 18. The studied UWB antenna prototype with a small-sized ridged cavity: (a) a plastic frame produced using SLA technology; (b) a plastic frame with an enamel coating; (c) an antenna with a plastic cavity that has an enamel coating.

well to the plots obtained during simulation; the deviations are insignificant and may be caused by inaccuracy in the manufacture of the prototype or inaccuracy in the calculations. The shapes of the measured radiation patterns (Figure 17) closely resemble those obtained in the simulation. Thus, the measurements validate all the simulation results.

5.2. UWB Antenna with Small-Sized Ridged Cavity

It is impossible to manufacture a small-sized cavity antenna frame with slots cut in the side walls using fused deposition modeling (FDM technology), as it does not have the precision and requires manual completion of the frame after printing the main part. Therefore, the frame is produced using SLA technology (Figure 18(a)). Foil application to this model is also not easy since high accuracy in replica copying of the prototype to the model is necessary, particularly at the area where the slots in the cavity walls are. Thus, the coating of the plastic frame is made with conductive enamel (Figure 18(b)). In all antenna configurations, enamel was hand-brushed painted with the resulting layer thickness not being even, and a conductive layer about 0.2 to 0.5 mm. To achieve a thinner and more uniform layer, enamel spraying can be used. After the enamel has been applied and cured, the active and passive exciters are placed on dielectric (nylon) and metal (brass) mounting racks, respectively. An SMA connector is mounted on the frame (cavity) using a nut, and the central conductor is soldered to the edge of the active exciter (Figure 18(c)).

For the manufactured prototype, the absolute reflection coefficient (Figure 19(a)) at the antenna input, gain (Figure 19(b)), and radiation patterns (Figure 20) were measured. The plots in Figure 19(b) show that the antenna gain almost corresponds to that obtained during simulation with the difference not exceeding 0.5 dB in the frequency band of 4–9 GHz. The antenna matching also corresponds to the plots obtained during simulation: there are some differences (frequency shift) in the curves shown in Figure 19(a), but they do not exceed 5%. This error is low and may be associated with both inaccuracy in the manufacture of the antenna elements or the entire assembly and inaccuracy in the full-wave simulation. The shapes of the measured radiation patterns (Figure 20) are close to the ones obtained in the simulation.

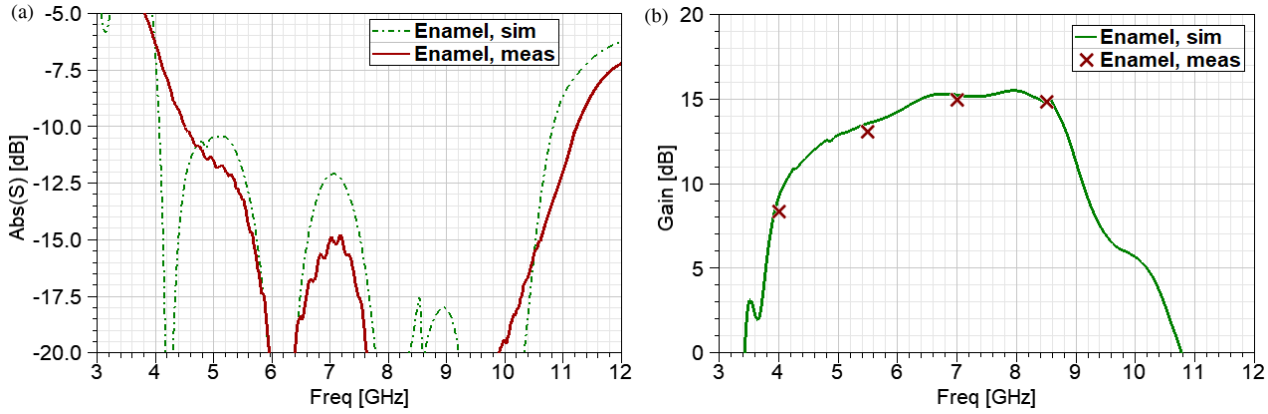

FIGURE 19. The results obtained of the UWB antenna with a small-sized two-layer ridged cavity: (a) the measured and simulated reflection coefficients; (b) the measured and simulated gain.

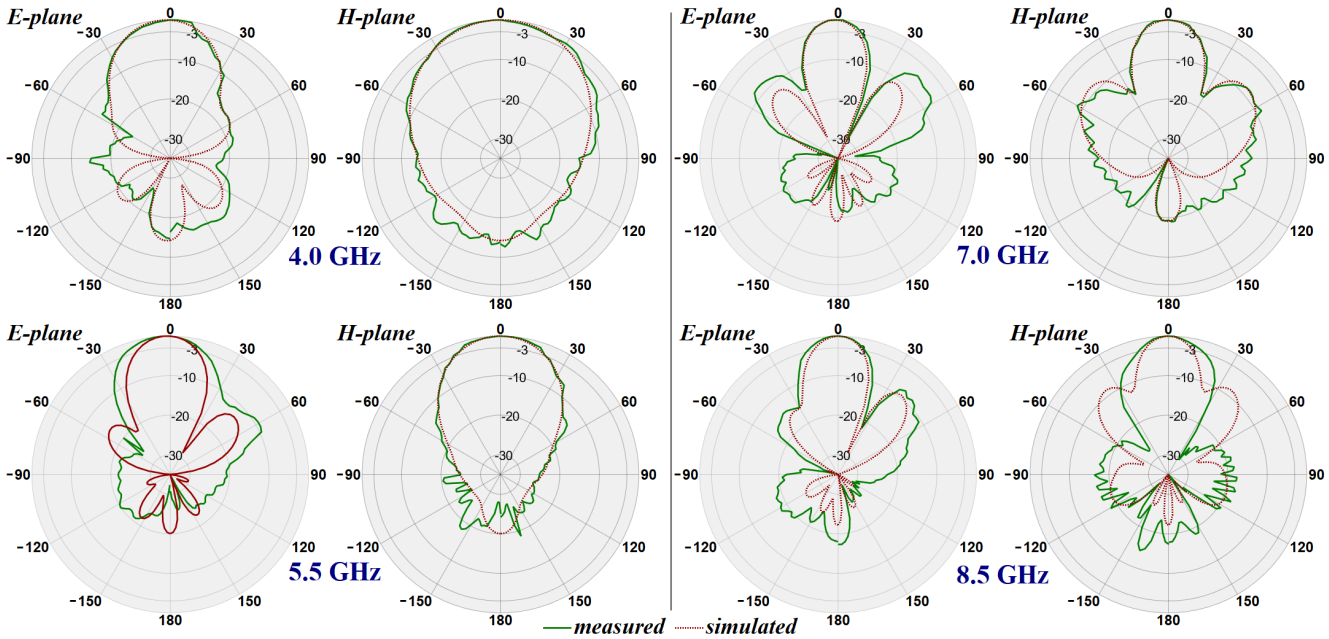

FIGURE 20. The radiation patterns of the proposed ultra-wideband small-sized two-layer ridged cavity antenna with enamel coating.

TABLE 1. Comparative characteristics of the proposed designs.

Antenna Type	Antenna with flat reflector	Antenna with large-sized cavity	Antenna with small-sized cavity
$BW_{G\geq 10\,dBi}$, GHz	4–8.8	3.8–9.6	4–9.2
$BW_{G\geq 10\,dBi}$, %	~ 75	~ 87	~ 79
Peak gain, dBi	13.5	18	15.8
Av. gain, dBi	~ 12.5	~ 15	~ 13.5
Peak AE, %	68	66	84
Av. AE, %	55–60	50–55	60–65
Overall size, mm^3	$90 \times 80 \times 10$	$125 \times 108 \times 21$	$85 \times 75 \times 10$

5.3. Discussions

The article examines three designs of UWB antennas. The first is a stacked microstrip antenna from [10] with a flat reflector (Figure 2(a)). The second type of antenna [10] is the one with a large-sized pyramidal cavity (Figure 2(b)), which allows for a significant increase in the antenna gain. And the third option is the antenna from [10] with the ridged small-sized pyramidal cavity (Figure 2(c)), where the design of the cavity allows increasing the gain without increasing the volume of the antenna (improving the aperture efficiency). Table 1 presents the com-

parative characteristics of the designs. The table shows that volumetric reflective structures significantly improve the radiation performance of antennas in wide and ultrawide frequency ranges, indicating the necessity and importance of research into such structures, particularly in terms of finding new methods of manufacturing antennas that are simpler and less expensive, simplifying and reducing the cost of the process.

Some previously published works describe the potential for manufacturing waveguides and horn antennas using 3D printing with a conductive coating [58–61], including those with complex shapes [62–63]. However, detailed studies on this method have not been conducted or published, particularly concerning the manufacture of reflectors or radiating elements of antennas. Therefore, the studies presented in this work are of great importance and relevance.

6. CONCLUSION

The article presents the results of calculations, simulations, and experimental measurements of cavity-backed ultra-wideband antennas, whose frames are made of dielectric materials (plastic) using 3D printing technology. This process incorporates a conductive layer made from either metal foil or enamel mixed with silver particles. The simulation results indicate that the application of thin conductive coatings does not reduce the radiation characteristics of the antenna compared to antennas with solid metal frames across the ultrawide frequency range of 3 to 12 GHz. Measurements derived from prototypes using these conductive coatings showed a high convergence with the simulation results. This reached the conclusion that the proposed manufacturing technique for antennas can be used in current antenna technology.

Due to the high performance, namely a gain exceeding 10 dBi across a frequency band greater than 80% with a matching level better than 10 dB and a radiation pattern oriented with the maximum along the normal to the plane of the antenna, the presented designs can be applied in various radio-measurement and radio-monitoring systems. With adjustments in the frequency range (and corresponding antenna sizes), these designs can also be useful in systems for the retransmission of mobile communications and signal amplification across both wide and ultrawide frequency ranges. Moreover, the reduction in manufacturing costs for such antennas makes them end-user-friendly.

Although the results were obtained from the reflective parts of antennas (such as cavities or volumetric reflectors), it can be supposed that this manufacturing technology is also applicable to the production of direct radiating elements or full-fledged antennas (for example, horn antennas). Future studies should be conducted to validate the effectiveness of this technology.

It is significant to note that the technology under investigation is remarkable for its potential to reduce the cost of antennas, production time, and design complexity. Therefore, the manufacturing of radiating elements using this technology seems impractical in the designs considered in this article. On the contrary, laser cutting of metal has become a user-friendly and cost-effective technology that enables the production of elements with highly precise dimensions. Among the promising areas for further research, we can highlight two key areas. The first is the production of radiating elements with complex shapes, where printing technologies or laser cutting cannot be applied (for example, spiral antennas of complex shapes or corrugated horns). Secondly, it is interesting to study the application of the exciter shapes on some dielectric objects, such as drawing a patch antenna on the body of an aircraft or satellite, including a flexible dielectric (RFID system).

ACKNOWLEDGEMENT

The radiation patterns and gains of the given UWB antennas were measured using equipment from the Ural Federal University's Center for Shared Use.

The author would like to express his sincere thanks to Kseniya Ivanchenko for her diligent proofreading of this paper.

REFERENCES

[1] Schantz, H. G., "Introduction to ultra-wideband antennas," in *IEEE Conference on Ultra Wideband Systems and Technologies, 2003*, 1–9, Reston, VA, USA, Nov. 2003.

[2] Milligan, T. A., *Modern Antenna Design*, John Wiley & Sons, 2005.

[3] Allen, B., M. Dohler, E. Okon, W. Malik, A. Brown, and D. Edwards, *Ultra-Wideband Antennas and Propagation: For Communications, Radar and Imaging*, John Wiley & Sons, 2007.

[4] Haraz, O. and A.-R. Sebak, "UWB antennas for wireless applications," *Advancement in Microstrip Antennas with Recent Applications*, 125–152, 2013.

[5] Chen, Z. N., D. Liu, H. Nakano, X. Qing, and T. Zwick, *Handbook of Antenna Technologies*, Springer, 2016.

[6] Kaur, K., A. Kumar, and N. Sharma, "A review of ultra wideband antennas with band notched characteristics," in *Proceedings of the International Conference on Innovative Computing & Communications (ICICC)*, 2020.

[7] Kumar, O. P., P. Kumar, T. Ali, P. Kumar, and S. Vincent, "Ultrawideband antennas: Growth and evolution," *Micromachines*, Vol. 13, No. 1, 60, 2022.

[8] Shishkin, M. S. and S. N. Shabunin, "Analysis of various designs of wideband patch antennas," in *2022 IEEE International Multi-Conference on Engineering, Computer and Information Sciences (SIBIRCON)*, 1190–1193, Yekaterinburg, Russian Federation, Nov. 2022.

[9] Shishkin, M. S., "Bandwidth enhancement methods analysis for high-gain stacked microstrip antenna," *Progress In Electromagnetics Research B*, Vol. 107, 19–31, 2024.

[10] Shishkin, M. S., "Ultrawideband high-gain stacked microstrip antenna with modified E-shaped active exciter and four single-sided bowtie passive elements," *Progress In Electromagnetics Research B*, Vol. 109, 1–16, 2024.

[11] Schulpen, R., U. Johannsen, S. C. Pires, and A. B. Smolders, "Design of a phased-array antenna for 5G base station applications in the 3.4-3.8 GHz band," in *12th European Conference on Antennas and Propagation (EuCAP 2018)*, 743, London, UK, Apr. 2018.

[12] Hua, C., R. Li, Y. Wang, and Y. Lu, "Dual-polarized filtering antenna with printed jerusalem-cross radiator," *IEEE Access*, Vol. 6, 9000–9005, 2018.

[13] Ushijima, Y., E. Nishiyama, and M. Aikawa, "Single layer extensible microstrip array antenna integrating SPDT switch circuit for linear polarization switching," *IEEE Transactions on Antennas and Propagation*, Vol. 60, No. 11, 5447–5450, 2012.

[14] Shishkin, M. S., "Wideband high-gain dual-polarized antenna for 5G communications," in *2021 XV International Scientific-Technical Conference on Actual Problems Of Electronic Instrument Engineering (APEIE)*, 311–316, Novosibirsk, Russian Federation, Nov. 2021.

[15] Shishkin, M. S., "Research of a wideband dual-polarization microstrip antenna array on a suspended substrate with irregular arrangement of elements," in *2024 IEEE 25th International Conference of Young Professionals in Electron Devices and Materials (EDM)*, 630–635, Altai, Russian Federation, Jul. 2024.

[16] Naji, D. K., J. S. Aziz, and R. S. Fyath, "Design and simulation of RFID aperture coupled fractal antennas," *International Journal of Engineering Business Management*, Vol. 4, 25, 2012.

[17] Vincenti Gatti, R., R. Rossi, and M. Dionigi, "Single-layer line-fed broadband microstrip patch antenna on thin substrates," *Electronics*, Vol. 10, No. 1, 37, 2021.

[18] Wen, L.-H., S. Gao, Q. Luo, Q. Yang, W. Hu, Y. Yin, X. Ren, and J. Wu, "A wideband differentially fed dual-polarized antenna with wideband harmonic suppression," *IEEE Transactions on Antennas and Propagation*, Vol. 67, No. 9, 6176–6181, 2019.

[19] Ou, N., X. Wu, K. Xu, F. Sun, T. Yu, and Y. Luan, "Wideband, dual-polarized patch antenna array fed by novel, differentially fed structure," *Electronics*, Vol. 13, No. 7, 1382, 2024.

[20] Wen, L.-H., S. Gao, Q. Luo, W. Hu, Q. Yang, Y. Yin, X. Ren, and J. Wu, "A wideband differentially driven dual-polarized antenna by using integrated six-port power divider," *IEEE Transactions on Antennas and Propagation*, Vol. 67, No. 12, 7252–7260, 2019.

[21] Li, Y., L. Wei, K. Wang, H. Cai, and Z. Chen, "Low-profile wideband dual-polarized patch antenna based on differential-paired multi-mode arms," *Electronics*, Vol. 12, No. 12, 2604, 2023.

[22] Ciydem, M. and E. A. Miran, "Dual-polarization wideband sub-6 GHz suspended patch antenna for 5G base station," *IEEE Antennas and Wireless Propagation Letters*, Vol. 19, No. 7, 1142–1146, 2020.

[23] Tang, H., X. Zong, and Z. Nie, "Novel broadband dual-polarized antenna for 5G applications," in *2018 International Symposium on Antennas and Propagation (ISAP)*, 1–2, Busan, Korea (South), 2018.

[24] Vadlamudi, R. and K. Sriram, "Nature stimulated dual band, dual polarized aerial with very good isolation for A-LTE/5G base station applications," in *2020 IEEE International Students' Conference on Electrical,Electronics and Computer Science (SCEECS)*, 1–3, Bhopal, India, 2020.

[25] Ta, S. X., D. M. Nguyen, K. K. Nguyen, C. D. Ngoc, and N. N. Trong, "Wideband differentially fed dual-polarized antenna for existing and sub-6 GHz 5G communications," *IEEE Antennas and Wireless Propagation Letters*, Vol. 19, No. 12, 2033–2037, 2020.

[26] Tu, Y., B. Feng, M. Wang, X. He, and Q. Zeng, "A three-element dual-polarized antenna array with beamwidth reconfiguration," in *2017 Sixth Asia-Pacific Conference on Antennas and Propagation (APCAP)*, 1–3, Xi'an, China, 2017.

[27] Gao, X., L. Zhang, Y. He, L. Zhang, W. Li, S.-W. Wong, and C.-H. Liao, "A dual-polarized compact patch antenna for sub-6 GHz 5G base stations," in *2020 IEEE Asia-Pacific Microwave Conference (APMC)*, 752–754, Hong Kong, 2020.

[28] Chen, Y., Y. He, W. Li, L. Zhang, S.-W. Wong, and A. Boag, "A 3-9 GHz UWB high-gain conformal end-fire Vivaldi antenna array," in *2021 IEEE International Symposium on Antennas and Propagation and USNC-URSI Radio Science Meeting (APS/URSI)*, 737–738, Singapore, Dec. 2021.

[29] Wang, Z., X. Zhao, F. Ji, S. Huang, and Z. Jiang, "Ultra-wideband cylindrical conformal array antenna based on LP-KDA," in *2020 IEEE MTT-S International Conference on Numerical Electromagnetic and Multiphysics Modeling and Optimization (NEMO)*, 1–4, Hangzhou, China, Dec. 2020.

[30] Midtbøen, V., K. G. Kjelgård, and T. S. Lande, "3D printed horn antenna with PCB microstrip feed for UWB radar applications," in *2017 IEEE MTT-S International Microwave Workshop Series on Advanced Materials and Processes for RF and THz Applications (IMWS-AMP)*, Pavia, Italy, Sep. 2017.

[31] Mahmud, R. H. and M. J. Lancaster, "A 2 × 2 filtering subarray element antennas using all-resonator structures," *IET Microwaves, Antennas & Propagation*, Vol. 15, No. 6, 592–599, 2021.

[32] Mahmud, R. H. and M. J. Lancaster, "High-gain and wide-bandwidth filtering planar antenna array-based solely on resonators," *IEEE Transactions on Antennas and Propagation*, Vol. 65, No. 5, 2367–2375, 2017.

[33] Jeong, T., J. Yun, K. Oh, J. Kim, D. W. Woo, and K. C. Hwang, "Shape and weighting optimization of a subarray for an mm-wave phased array antenna," *Applied Sciences*, Vol. 11, No. 15, 6803, 2021.

[34] Sun, D., W. Dou, and L. You, "Application of novel cavity-backed proximity-coupled microstrip patch antenna to design broadband conformal phased array," *IEEE Antennas and Wireless Propagation Letters*, Vol. 9, 1010–1013, 2010.

[35] Kong, D. K., J. Kim, D. Woo, and Y. J. Yoon, "Broadband modified proximity coupled patch antenna with cavity-backed configuration," *Journal of Electromagnetic Engineering and Science*, Vol. 21, No. 1, 8–14, 2021.

[36] Klemm, M., I. J. Craddock, J. A. Leendertz, A. Preece, and R. Benjamin, "Radar-based breast cancer detection using a hemispherical antenna array — experimental results," *IEEE Transactions on Antennas and Propagation*, Vol. 57, No. 6, 1692–1704, 2009.

[37] Elsherbini, A., J. Wu, and K. Sarabandi, "Dual polarized wideband directional coupled sectorial loop antennas for radar and mobile base-station applications," *IEEE Transactions on Antennas and Propagation*, Vol. 63, No. 4, 1505–1513, 2015.

[38] Zhang, Y., S. Lin, L. Wang, and Q. Ding, "A wideband dual-cavity-backed polarization reconfigurable antenna based on liquid metal switches," *Progress In Electromagnetics Research Letters*, Vol. 108, 75–83, 2023.

[39] Fan, J., J. Lin, J. Cai, and F. Qin, "Ultra-wideband circularly polarized cavity-backed crossed-dipole antenna," *Scientific Reports*, Vol. 12, No. 1, 4569, 2022.

[40] Yang, J. O., S. Bo, J. Zhang, and F. Yang, "A low-profile unidirectional cavity-backed log-periodic slot antenna," *Progress In Electromagnetics Research*, Vol. 119, 423–433, 2011.

[41] Di Paola, C., K. Zhao, G. F. Pedersen, and S. Zhang, "Multi-mode dual-polarised cavity backed patch antenna array for 5G mobile devices," *IET Microwaves, Antennas & Propagation*, Vol. 15, No. 3, 280–288, 2021.

[42] Chaloun, T., P. Grüner, and W. Menzel, "Design and analysis of a novel wide-angle scanning stub-loaded cavity array element," *IEEE Open Journal of Antennas and Propagation*, Vol. 3, 783–797, 2022.

[43] Cao, B., H. Wang, J. Zheng, and Y. Huang, "High-gain substrate integrated cavity antenna array with laminated waveguide feeding network for W-band application," in *2015 European Microwave Conference (EuMC)*, 1049–1052, Paris, France, Sep. 2015.

[44] Baard, C., Y. Liu, and N. Nikolova, "Ultra-wideband low-cost high-efficiency cavity-backed compound spiral antenna," *Electronics*, Vol. 9, No. 9, 1399, 2020.

[45] Gupta, E., C. Bonner, F. Muhammed, K. McParland, and M. Mirotznik, "Design and fabrication of multi-material broadband electromagnetic absorbers for use in cavity-backed antennas," *Heliyon*, Vol. 9, No. 3, e14164, 2023.

[46] Bai, X. and S.-W. Qu, "Wideband cavity-backed crossed dipoles for circular polarization," *Progress In Electromagnetics Research Letters*, Vol. 36, 133–142, 2013.

[47] Zhang, Z.-Y., S. Zuo, X. Zhang, and G. Fu, "Ultra-wideband cavity-backed bowtie antenna for pattern improvement," *Progress In Electromagnetics Research Letters*, Vol. 37, 37–46, 2013.

[48] Li, T., "Dual circularly polarized substrate integrated waveguide cavity-backed antenna with enhanced bandwidth and reduced size for wideband wireless applications," *Progress In Electromagnetics Research M*, Vol. 84, 117–126, 2019.

[49] Shishkin, M. S., "Aperture efficiency improvement methods analysis for high-gain wideband/ultrawideband stacked microstrip antennas," in *2024 IEEE 3rd International Conference on Problems of Informatics, Electronics and Radio Engineering (PIERE)*, 260–265, Novosibirsk, Russian Federation, Nov. 2024.

[50] Galejs, J., "Admittance of a rectangular slot which is backed by a rectangular cavity," *IEEE Transactions on Antennas and Propagation*, Vol. 11, No. 2, 119–126, 1963.

[51] Long, S., "Experimental study of the impedance of cavity-backed slot antennas," *IEEE Transactions on Antennas and Propagation*, Vol. 23, No. 1, 1–7, 1975.

[52] Long, S., "A mathematical model for the impedance of the cavity-backed slot antenna," *IEEE Transactions on Antennas and Propagation*, Vol. 25, No. 6, 829–833, 1977.

[53] Raha, K. and K. P. Ray, "A high gain, wide bandwidth and low cross-polarization compact horn antenna fed by a cavity-backed stacked microstrip antenna," *Progress In Electromagnetics Research C*, Vol. 132, 231–240, 2023.

[54] Hong, J.-S., *Microstrip Filters For RF/Microwave Applications*, John Wiley & Sons, 2011.

[55] Garg, R. and I. Bahl, *Microstrip Lines and Slotlines*, Artech House, 2024.

[56] Horton, R., B. Easter, and A. Gopinath, "Variation of microstrip losses with thickness of strip," *Electronics Letters*, Vol. 7, No. 17, 490–491, 1971.

[57] Garg, R., K. C. Gupta, and R. Sharan, "Optimum thickness of metal in waveguiding structures, ground planes and reflectors," *International Journal of Electronics Theoretical and Experimental*, Vol. 39, No. 5, 525–527, 1975.

[58] Hoel, K. V., S. Kristoffersen, J. Moen, G. Holm, and T. S. Lande, "Characterization of a 3D printed wideband waveguide and horn antenna structure embedded in a UAV wing," in *2016 10th European Conference on Antennas and Propagation (EuCAP)*, 1–4, Davos, Switzerland, Apr. 2016.

[59] Hoel, K. V., S. Kristoffersen, J. Moen, K. G. Kjelgård, and T. S. Lande, "Broadband antenna design using different 3D printing technologies and metallization processes," in *2016 10th European Conference on Antennas and Propagation (EuCAP)*, 1–5, Davos, Switzerland, Apr. 2016.

[60] Geterud, E. G., P. Bergmark, and J. Yang, "Lightweight waveguide and antenna components using plating on plastics," in *2013 7th European Conference on Antennas and Propagation (EuCAP)*, 1812–1815, Gothenburg, Sweden, Apr. 2013.

[61] Périgaud, A., S. Bila, O. Tantot, N. Delhote, and S. Verdeyme, "3D printing of microwave passive components by different additive manufacturing technologies," in *2016 IEEE MTT-S International Microwave Workshop Series on Advanced Materials and Processes for RF and THz Applications (IMWS-AMP)*, 1–4, Chengdu, China, Jul. 2016.

[62] Majumdar, B., D. Baer, S. Chakraborty, K. P. Esselle, and M. Heimlich, "A 3D printed dual-ridged horn antenna," in *2016 International Conference on Electromagnetics in Advanced Applications (ICEAA)*, 836–839, Cairns, QLD, Australia, Sep. 2016.

[63] Midtbøen, V., K. G. Kjelgård, and T. S. Lande, "3D printed horn antenna with PCB microstrip feed for UWB radar applications," in *2017 IEEE MTT-S International Microwave Workshop Series on Advanced Materials and Processes for RF and THz Applications (IMWS-AMP)*, 1–3, Pavia, Italy, Sep. 2017.